Probing structural evolution along multidimensional reaction coordinates with femtosecond stimulated Raman spectroscopy

Renee R. Frontiera[1], Chong Fang[2], Jyotishman Dasgupta[3] and Richard A. Mathies[4]*

[1]Department of Chemistry, Northwestern University, Evanston, IL 60208

[2]Department of Chemistry, Oregon State University, Corvallis, OR, 97331

[3]Department of Chemistry, Tata Institute for Fundamental Research, Mumbai, India, 400005

[4]Department of Chemistry, University of California, Berkeley, CA 94720

Submitted as an invited review to *Physical Chemistry Chemical Physics*

*Corresponding author

Email: ramathies@berkeley.edu

Phone: (510) 642-4192

Fax: (510) 642-3599

Abstract

Mapping out multidimensional potential energy surfaces has been a goal of physical chemistry for decades in the quest to both predict and control chemical reactivity. Recently a new spectroscopic approach called Femtosecond Stimulated Raman Spectroscopy or FSRS was introduced that can structurally interrogate multiple dimensions of a reactive potential energy surface. FSRS is an ultrafast laser technique which provides complete time-resolved, background-free Raman spectra in a few laser shots. The FSRS technique provides simultaneous ultrafast time (~50 fs) and spectral (~8 cm^{-1}) resolution, thus enabling one to follow reactive structural evolutions as they occur. In this perspective we summarize how FSRS has been used to follow structural dynamics and provide mechanistic detail on three classical chemical reactions: a structural isomerization, an electron transfer reaction, and a proton transfer reaction.

Introduction – A new window on chemical reactivity

Chemical reactivity is determined by the potential energy landscape of the reacting species. Mapping this landscape and the dynamics that occur upon it has been a goal of physical chemistry over the past century, as revealing even small portions of the potential energy surface advances our understanding significantly, leading to accurate predictions of the rate and outcome. However, in order to fully understand a potential energy surface (PES), one must measure or calculate the instantaneous frequency, population and anharmonicities of all of the relevant vibrational modes at every point on the surface. This multidimensional hypersurface, in which the number of dimensions is given by the number of nuclear coordinates involved in the reaction, can be extremely complex.[1, 2]

The complexity of these hypersurfaces has been visualized by both experimental and theoretical means, but for large molecules such as proteins, a precise picture is still daunting. Excellent theoretical approaches to this problem have provided some of the best insights to date on the nature of multidimensional potential energy surfaces.[3, 4] Experimental approaches generally lack the structural and temporal resolution needed for a critical comparison. Towards this end we will focus in this review on mapping and understanding multidimensional reactions using the technique called Femtosecond Stimulated Raman Spectroscopy (FSRS), which is starting to open an exciting new window on chemical reactivity.

FSRS is an ultrafast vibrational technique which is capable of obtaining complete Raman vibrational spectra with sub-100 fs time resolution.[5-9] By examining the structure of a reacting species on the time scale of reactive vibrational motion, we are able to

follow many of the nuclear changes along the reaction coordinate, thus mapping out this important region of the potential energy surface. The experimental advantages of the FSRS technique[10] as well as a complete theoretical analysis[11-13] have been presented previously. Applications of FSRS have been rapidly expanding as groups worldwide performed studies on such wide-ranging problems as microscopy,[14] intramolecular electron transfer[7] and stilbene dynamics.[15] Here we focus on three paradigmatic chemical reactions - an excited state isomerization,[16] an electron transfer reaction,[17] and proton transfer in the green fluorescent protein (GFP)[18] - that illustrate how we can advance our understanding of chemical reaction dynamics with this new spectroscopy.

As shown in Figure 1, FSRS is a three-pulse laser technique, involving two femtosecond pulses (the actinic pump and probe pulses) and one picosecond pulse (the Raman pump pulse). The beams are non-collinearly focused into the sample, and the heterodyned signal follows the probe beam direction. The three beams excite the sample and then interrogate the structure by acquiring a stimulated Raman spectrum at some time delay after excitation. The sample is promoted from the ground to the excited state by exciting in its absorption band with the femtosecond actinic pulse. After some time delay, a pair of interactions with the Raman pump and probe pulses creates a vibrational coherence in the sample. During the vibrational polarization free induction decay (FID), there is another interaction with the picosecond Raman pulse, and a Raman shifted photon is emitted in the probe direction. FSRS is an intrinsically heterodyned technique, and Raman photons are detected on top of the probe spectrum. By dividing subsequent laser shots with the Raman pump on and off, a background free Raman spectrum is obtained. Spectra of cyclohexane which are the difference (top) of the Raman pump-off

spectra from the Raman pump-on spectra, and the ratio (bottom) of the spectra, are shown in Figure 1. Division of the spectra rather than subtraction ensures that the signal magnitude, reported as a percent Raman gain, is independent of probe laser power.

The timing precision in the experiment is given by the cross correlation of the actinic pump and the probe pulse, and can be as short as ~ 10 fs with an appropriate laser system. The first pair of Raman interactions can only occur when the femtosecond probe is on the sample, so the vibrational coherence is initiated with excellent time precision. The uncertainty principle is not violated in this process, since the second upward interaction with the Raman pump can occur at any time during the FID, and the emitted photons are not temporally detected. Thus, for a molecule in which the vibrational frequencies do not change during the dephasing of the vibration, the time resolution can be ~ 10 fs with excellent spectral resolution.

The usual assumption that the experimental time resolution is determined by the cross correlation time can be misleading, as the vibrational structure can change during the dephasing time.[19, 20] Conceptually, this could be depicted as a shift or oscillation in the horizontal lines which represent the vibrational energy levels in Figure 1. A rapid change in frequency or an oscillatory perturbation from another mode could affect the vibrational frequency and/or intensity during the vibrational dephasing process. This will result in changes in the lineshape, frequency, and/or intensity of the detected vibrational modes in a FSRS experiment, and can be modeled to reveal structural changes that occur faster than the vibrational dephasing time. It is important to note that this circumstance does not alter the intrinsic time resolution of the experiment, but does enhance the interpretation.

The experimental advantages of the FSRS technique include the relative ease of use, rapid data acquisition times, and excellent signal to noise (S/N) ratios. Only 3 non-phase-locked pulses are required to monitor excited state structure, and with the development of kHz readout CCD detectors, complete high S/N vibrational spectra spanning over 2000 cm^{-1} can be recorded in a single pair of shots, or just 2 milliseconds with a kHz amplifier. The signals are also free from fluorescence due to the stimulated nature of detection, and unlike infrared spectroscopy, can easily be used to measure vibrational structure in aqueous solutions.

Previously these unique advantages have enabled the acquisition of structural information in a wide variety of systems, including bacteriorhodopsin,[21, 22] rhodopsin,[23] and carotenoids.[24] Here we present recent examples which detail the ways in which FSRS may be used to examine portions of the multidimensional potential energy surface in three classical chemical reaction processes. We begin with a structural rearrangement reaction - the isomerization of the tetrapyrrole chromophore in phytochrome, followed by electron transfer between dye molecules and titanium dioxide nanoparticles, and conclude with the vibrationally mediated proton transfer reaction in the green fluorescent protein (GFP). These reactions are typical of many photoreactions in chemistry and biology and illustrate the versatility of FSRS while simultaneously pointing the way to future investigations.

Excited state isomerization in phytochrome

Phytochrome is a light sensing protein found in higher plants and bacteria which is responsible for light sensing and maturation responses.[25] The bilin chromophore, which consists of four pyrrole rings, is conserved across all phytochromes, and the proposed structures for the cyanobacterial red-absorbing (P_r) and far red-absorbing (P_{fr}) forms are depicted in Figure 2. The light sensing process involves a photoisomerization which flips the orientation of the D ring of the chromophore.

In considering the PES of the phytochrome isomerization reaction, a key question is determining at which point the isomerization actually occurs. As the isomerization of phytochrome is a photoreaction, the excited electronic surface clearly plays an important role in initiating the chemistry, but in some photoreactions, most notably rhodopsin, the majority of nuclear changes occur on the ground state surface following very fast excited state dynamics.[23] In phytochrome, a Strickler-Berg analysis of the fluorescence from P_r indicates that the excited state lifetime is 28 ps,[26] a number which is supported by transient absorption measurements. These data suggest that the excited state lifetime is easily long enough to accommodate isomerization but direct structural measurements are required to test this hypothesis.

Figure 3 displays the time-resolved FSRS spectra following photoexcitation for the P_r to P_{fr} transition in Cph1 phytochrome. Representative spectra[16] at 0.6, 3 and 40 ps are displayed, and ground state spectra of both species are included for comparison. Especially the C=C stretch frequencies, the C-C stretch, and the HOOP intensity and frequency show that the 3 ps spectrum is nearly identical to that at 40 ps, and that of the ground state P_{fr} chromophore. Thus, FSRS has shown that the isomerization reaction is

essentially complete by 3 ps, and that this isomerization occurs on the excited state surface. The 3 ps spectrum is thus assigned to the Lumi-R* state, which decays to the Lumi-R state with a time constant of 30 ps. Interestingly, the chromophore structure does not noticeably change in this decay process.

With the intrinsic high time resolution of FSRS, it is also possible to observe the structural changes that occur *during* this isomerization. The 0.6 ps spectrum captures a structural snapshot on the excited state surface as the D ring is rotating. This rotation is evidenced by the large Raman intensity in the hydrogen out-of-plane (HOOP) mode at 816 cm^{-1}, which arises because the planarity of the methyne bridge between the C and D rings is broken by the rotation. This mode downshifts in frequency as the P_{fr} structure is established, and has dropped to 806 cm^{-1} by 3 ps. There is a further downshift in frequency to 803 cm^{-1} at 40 ps, as the chromophore relaxes and cools in the Lumi-R state. Thus the majority of the structural evolution of the chromophore occurs by 3 ps.

Additionally, we can quantify the excited state population by probing the magnitude and decay of the excited state features as a function of time. There is a partitioning on the excited state surface quite early in the photo-reaction, at 3 ps, which results in a large portion (85%) of the initially excited molecules returning to the P_r ground state.[16] This surprisingly large return means that the quantum yield of the overall reaction, which takes milliseconds and involves large conformational changes of the protein, is determined in the first few picoseconds of evolution on the excited state surface. This partitioning is likely due to the steric collision of the rotating D ring chromophore with protein residues in the binding site during the early stages of the reaction.

Our conclusion that the isomerization in phytochrome primarily occurs on the excited state surface would not be possible without the insight provided by a time-resolved structural technique. While the lifetimes of the various states were known from transient absorption measurements, the structural changes and quantum yields involved at various time points in this photoreaction were unknown. With the structural data provided by FSRS, it is possible to prove that the isomerization occurs much more quickly than previously expected, and does so on the excited state surface. We expect that FSRS will be increasingly useful in determining the structural differences between many reaction intermediates found in the ubiquitous *cis-trans* isomerizations in photochemistry and photobiology.[15, 27]

Nuclear dynamics of interfacial electron transfer

FSRS has also been used to probe the nature of interfacial electron transfer in dye-nanoparticle conjugate systems. Classical electron transfer theory,[28] which considers the effects of one or at most two[29] vibrational or nuclear motions in promoting electron transfer, has reduced the problem of the multidimensional potential energy surface to a restricted model system. While highly successful in predicting rates of some types of electron transfer reactions, this approach loses focus on the explicit nuclear degrees of freedom which promote electron transfer. Additionally, in some circumstances, particularly the ultrafast and efficient electron transfer processes utilized in photovoltaic devices, it is challenging to predict rates and reactivity using conventional theories. Since nuclear motions likely gate ultrafast electron transfer, in order to fully understand the reaction and predict reactivity, it is necessary to examine the multiple atomic motions

which drive the reaction, thus mapping out the reaction's multidimensional potential energy surface.

Interfacial electron transfer (IET), which in our experiments is focused on charge injection from a dye molecule into a titanium dioxide nanoparticle, is an interesting case as the electron is injected into the acceptor conduction band, rather than into an individual molecular state, as shown in Figure 4. Rapid movement along the excited D*-A surface brings the wavepacket to the charge transfer D^+A^- band. Since the modes that promote these reactions have never been determined, this potential energy surface is usually depicted as a simple one-dimensional harmonic oscillator. Such systems are commonly used in the fabrication of dye sensitized solar cells,[30] so understanding the nuclear motions which drive the wavepacket down the D*A surface is extremely important. Rapid and efficient electron transfer typically leads to solar cells with increased efficiency. Thus, understanding the multiple vibrational modes and nuclear motions which promote electron transfer will enable synthetic insights that improve the efficiency of these cheap and flexible cells.

The FSRS technique, which has the additional experimental advantages of significantly reduced fluorescence and Rayleigh scattering as compared to conventional Raman measurements, is valuable in looking at dye and particle systems, such as Coumarin 343 (C343)-conjugated titania nanoparticles. Previous transient absorption work on colloidal C343-TiO_2 identified a 100-200 fs component to the charge injection process and a 230 ps charge recombination time.[31-33] However in these transient absorption experiments it is difficult to obtain information other than the timescales of charge injection and back electron transfer; electronic absorption is typically insensitive

to vibrational structure and suffers from overlapping absorption bands making assignments challenging.

Two different stimulated Raman experiments were performed on these samples in order to identify structural rearrangements at different points in the reaction. First, resonance ground state FSRS, which uses only the Raman pump and probe pulses, can be used to identify modes which drive the complexes out of the initial Franck-Condon region on the excited state surface.[34-37] Since the transfer occurs on a rapid ~100 fs timescale, it is logical to assume that these initial motions out of the Franck-Condon region are those that drive the electron transfer process.

The ground state resonance FSRS spectra of the Coumarin 343-TiO_2 complex are shown in Figure 5. The enhancement of at least 10 vibrational modes proves the necessity of considering much more than two nuclear degrees of freedom in these types of electron transfer processes. Additionally, the character of these modes illuminates the mechanism of the IET process. All enhanced modes involve stretching of the carbon p-backbone, and no predominately nitrogen stretching modes are enhanced. This indicates that the donated electron comes from the pi-bonding backbone, rather than the nitrogen center. Additionally, coordinated motion from many of these carbon atoms is required to catalyze this ultrafast electron transfer process.

Further information on this charge-transfer complex comes from the resonance enhancement of various Ti-O stretching modes around 500 cm^{-1}. Due to the nature of the resonance enhancement effect, these modes arise from the direct binding of the carboxylic acid foot on the Coumarin molecules to the titania surface. The large cluster of Ti-O modes is indicative of heterogeneous binding conditions, likely due to surface

defects on the nanoparticles. FSRS experiments with controlled surfaces are called for to determine the binding structure directly.

To study structure and dynamics following of charge transfer photoexcitation, we performed a three pulse FSRS experiment which examined the structural evolution of the C343-TiO_2 complex. The vibrational spectrum corresponding to the ground state radical cation of C343 is shown in Figure 6. Although noisy due to the lack of resonance enhancement, the spectrum clearly and reproducibly shows three peaks at 1205, 1358, and 1549 cm^{-1}, corresponding to the CH_2 rocking, in plane H rocking, and C=C stretching modes. Comparing the frequency of these peaks to calculated DFT frequencies, we conclude that the hole is delocalized and resides on the carbon backbone of C343. By monitoring the kinetics of the 1549 cm^{-1} peak, we determined the decay of this radical cation species. The cation exhibits a characteristic rise time of 140 fs, and its decay is best fit to two time constants of 1.2 ps and 250 ps. The long time constant agrees with transient absorption measurements for back electron transfer from the nanoparticle into the dye molecule, and the shorter time constant is most likely due to electron transfer from unbound coumarin dye molecules into the radical cation bound coumarin molecules.

These experiments present one of the first uses of a vibrational structural technique to examine an ultrafast interfacial electron transfer process, and suggest the opportunity of exploiting structural measurements for rational design. Our vibrational data confirm the direct binding of the carboxylic acid foot to the TiO_2 nanoparticles, and future experiments could identify the exact nature of the binding. Additionally, we have proven that electron donation occurs from the pi bonding system near the nanoparticle, and involves concerted motion of many of these vibrational modes. Future experiments

with higher time resolution will track the evolution of these modes over time during the actual electron transfer process. This should lead to great improvements in our understanding and modeling of these reactions, and should at last reveal the nuclear coordinates which facilitate the electron transfer process.

Multidimensional reaction coordinate for proton transfer in GFP

The remarkably efficient fluorescence of the Green Fluorescent Protein (GFP) has lead to countless biological advances, due to its use as a biomolecular fluorescent label and genetic tag.[38-40] The fluorescence comes from the hydroxybenzylidene-imidazolinone chromophore which is formed by cyclization of sequential serine, tyrosine, and glycine residues within the beta-barrel of the protein.[41] Significant work by many groups[42-49] has proven that the fluorescence results from the anionic I^* state of the chromophore in an unrelaxed protein environment, which is formed after an excited-state proton transfer process following UV excitation of the neutral A species. This reaction is remarkably efficient, in that 80% percent of absorbed photons result in the emission of fluorescence. However, as most of the ultrafast studies on GFP relied on transient absorption experiments, the mechanistic details behind this efficient proton-transfer remained unknown. Since a proton-transfer chain reaction is likely to involve changes of at least several heavy nuclear coordinates in addition to proton motion, it is critical to examine the reaction with a vibrational structural technique in order to determine the mechanistic origin of the remarkable fluorescence. Additionally, the intrinsic rapidity of proton motion as compared to other molecular motions provides a unique opportunity for timescale separation to observe reaction gating by heavy atom vibrations.

To examine the multidimensional reaction coordinate in the GFP proton transfer reaction, FSRS was used to probe the initially prepared wavepacket's journey from the Franck-Condon region (A*) to the fluorescent species (I*).[18] Due to the resonance enhancement conditions of the experiment the A* vibrations dominate the spectra, and no features from the protein, ground state, or I* vibrations are seen. These time-resolved spectra and structural assignments are displayed in Figure 7, which plots the evolution of the vibrational features immediately following photoexcitation. Peaks at 1145 and 1190 cm^{-1} are attributed to primarily phenol C-H rocking motions, and the peaks at 1405, 1450, and 1565 cm^{-1} are the C-N and C=N stretching modes. The peak at 1270 cm^{-1} is the C-O stretch, which is highly sensitive to the degree of protonation of the phenol ring.

Surprisingly, Figure 7 shows that these peaks oscillate in intensity as time passes following photoexcitation. Even more remarkable is that the oscillations are out-of-phase for modes localized on opposite rings of the chromophore. For example, the C-N and C=N modes on the imidazolinone ring are at a maximum in intensity at a time delay of 500 fs, but the phenolic modes are at a minimum in intensity. The oscillations are cyclic with a period of ~280 fs. This out-of-phase behavior for the intensity oscillations on the two rings rules out any experimental artifacts for this signal, and indicates that the electron density is moving back and forth between the two rings. The molecule is evidently perturbed by a low frequency mode with a period of 280 fs; the mode modulates the electron density in the two rings, which results in a modulation of the molecular polarizabilities and the intensity of the Raman signal. As might be expected for a periodic modulation of electron density, the frequencies of these modes are also

perturbed and the modes on opposite chromophore rings oscillate in an out-of-phase manner.[18]

These out-of-phase oscillations in intensity and frequency demonstrate that a certain low frequency mode is modulating the molecular structure of the two rings. According to DFT calculations on the chromophore, there is a ~120 cm^{-1} (period = 280 fs) two-ring out-of-plane wagging mode, which brings the phenolic proton in and out of hydrogen bonding distance with the Wat22 oxygen atom (depicted in Fig. 8). This mode thus periodically arranges the position of the heavy chromophore atoms to facilitate a favorable proton transfer environment. We conclude that the wagging vibrational mode gates the excited-state proton transfer reaction, resulting in the highly efficient proton transfer and subsequent fluorescence process.

A depiction of the overall proton transfer reaction is presented in Figure 9. Upon initial excitation, the high frequency O-H stretch oscillates, attempting to surmount the proton transfer potential barrier. The impulsively excited low frequency ring wagging mode periodically brings the phenolic ring into better hydrogen bonding alignment with a nearby water molecule, thereby lowering the proton transfer barrier. After a certain number of oscillations, more of the heavy atoms in the hydrogen bonded chain have shifted position, and the wavepacket finally crosses over the proton transfer barrier. The ring wagging motions bring the phenolic hydrogen approximately half of the way towards complete proton transfer, catalyzing the tautomerization.

Using the FSRS technique, we were able to see the effects that this low frequency wagging mode has on the other vibrational frequencies; thus directly measuring the anharmonic coupling which shapes this potential energy surface along the reaction

coordinate. It is crucial to realize that the proton transfer reaction coordinate in GFP is not dominated by changes in the O-H stretching coordinates, which is all that would be suggested by a one-dimensional picture. Instead, many displacements by the non-hydrogen atoms are required to make a stable deprotonated species. In this work we have identified the primary gating motion, the low frequency ring wagging vibration, which enables these necessary atomic changes and thus produces a stable system with a deprotonated phenol group. More generally we conclude that studying complex photoreactions, particularly in proteins and in condensed phase environments, requires careful consideration and accurate measurement of all nuclear coordinates in order to understand their rate, mechanism and product.

Prospects for enhanced studies of reactivity

No discussion on mapping potential energy surfaces would be complete without considering the interplay between vibrations and vibrational coupling. Without vibrational coupling, all surfaces would be bound and nearly harmonic, and mapping the potential energy surface would be trivial. However, this would be quite an uninteresting world as it is the frequency changes, anharmonicity, and vibrational couplings that determine chemical reactivity and the photochemical functionality of the primary reactions on our planet.

Several attempts have been made to extend the FSRS technique into the realm of multidimensional spectroscopy to expose these anharmonicities. One promising attempt involved the detection of what were initially thought to be frequency modulated anharmonic coupling signals driven by impulsive excitation of low frequency vibrational

modes. In these experiments, detailed in references [50-53], oscillating sidebands are seen off of the high frequency modes. The energy spacing and temporal oscillation of the sidebands correspond to the impulsively excited low frequency modes. By modeling these signals with a coupled-wave description of FSRS, it was concluded that the sidebands resulted from a frequency modulation caused by anharmonic coupling. Later quantum mechanical theoretical work supported this conclusion, although the magnitudes of the experimental and theoretical sideband signals were not compared.[54]

Recent work by McCamant *et al.* [52, 53] has shown that these sidebands are actually the result of third-order cascading signals, rather than the desired fifth-order anharmonic coupling signals. Elegant experiments using a mixture of solvents revealed that the sideband signals were not limited to vibrational modes of one molecular species, but rather were seen from all molecular species. This disappointing result is not new in fifth-order Raman experiments. Promising work by Tokmakoff and Fleming in 1997[55], as well as several other groups[56-58], were thought to have measured the intermolecular force-force correlation function in CS_2 using fifth-order Raman. However, discrepancies in the theoretical and experimental results led to the conclusion, in 1999[59], that the signals were dominated by a cascading third-order process, and an upper limit of 2% was placed on the fifth-order signal.

An alternative approach for exploring anharmonicity in multidimensional reaction dynamics could come from performing FSRS with higher time resolution pump and probe pulses. In our original GFP experiments, wavepackets were only created in low frequency (< 300 cm^{-1}) modes due to the limited bandwidth of our actinic pulse, and we detected the influence of these wavepackets in driving the chemical reaction. However,

higher frequency modes undoubtedly play a role in this and all other chemical reactions. By using broadband pulses as short as 5 fs[60, 61] which would excite coherences in all heavy atom modes during photoexcitation, their effects should be observed as multi-sinusoidal oscillations in the frequency and/or intensity of coupled modes. Figure 10 presents a schematic representation of the data which might result from such an experiment: numerous modes would exhibit frequency and intensity oscillations, the extent of which would determine the degree of vibrational coupling. The key experimental challenges would be measuring these high frequency oscillations during the FSRS coherence time; however, the Raman pump pulse could be artificially truncated in time in order to detect oscillations. Thus, by monitoring the time-dependent couplings between all Raman active vibrational modes, a significant portion of the multidimensional potential energy surface along the reaction coordinate could be experimentally measured, leading to unprecedented advances in our understanding of chemical reaction dynamics.

Conclusion

Mapping multidimensional potential energy surfaces experimentally has been a dream for decades.[62-64] The FSRS experiments described here demonstrate that a variety of chemical reactions can now be examined to expose the multidimensionality of their reaction coordinate. Prompted by these results and exploiting access to steadily improving laser technology, we predict that FSRS will ultimately provide a wealth of new information on reaction coordinates and potential energy surfaces.

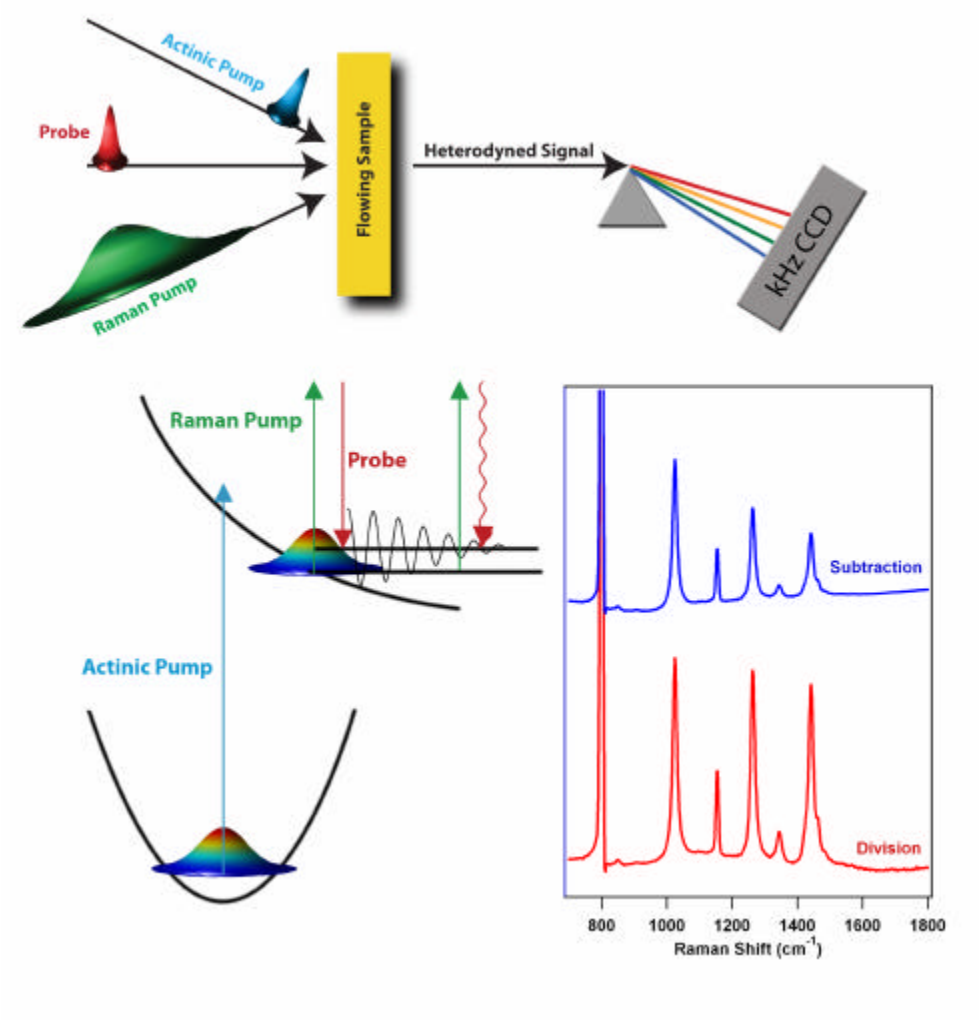

Figure 1. Schematic experimental setup of a time-resolved FSRS experiment. The femtosecond actinic pump pulse first photoexcites the sample. Then, focusing on the dominant time ordered diagram, after some time delay the femtosecond probe pulse and picosecond Raman pump pulse interrogate the instantaneous molecular structure. The self-heterodyned signal is emitted in the probe direction, dispersed, and detected by a kHz readout CCD. Data collection is best performed by division of subsequent Raman pump-on by Raman pump-off laser shots (red trace), but has been performed by other groups as a subtraction of subsequent pulses (blue). Subtraction leads to Raman amplitudes which undesirably depend on the probe power and spectral shape.

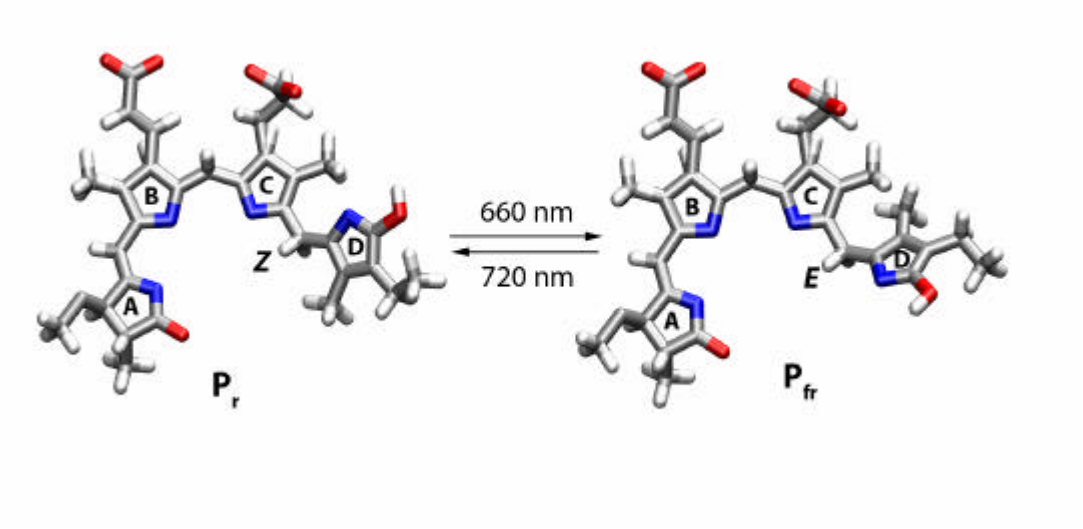

Figure 2. Structure of the phytochrome bilin chromophore in the Cph1 protein binding pocket.[16, 65] The P_r to P_{fr} transition involves an isomerization about the C_{14}=C_{15} bond which rotates the D ring.

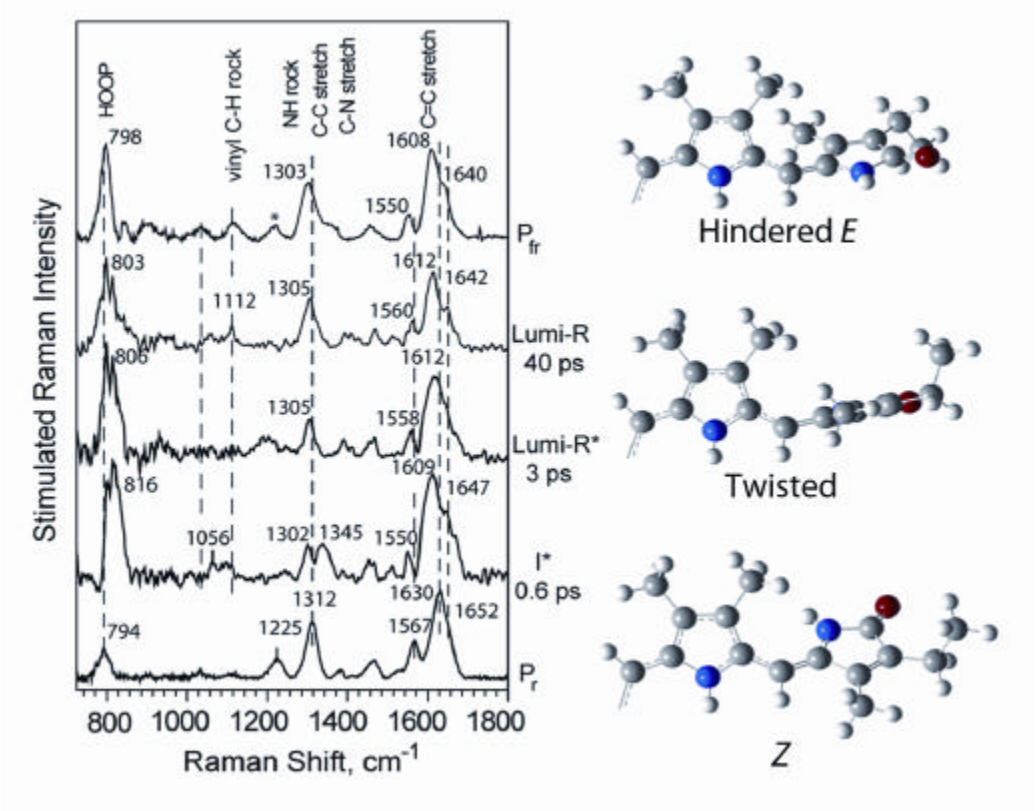

Figure 3. Femtosecond stimulated Raman spectra of the P_r to P_{fr} isomerization in phytochrome. Left: Representative spectra at the 0.6, 3 and 40 ps time delays, corresponding to the I*, Lumi-R* and Lumi-R states, respectively. Ground state spectra of P_r and P_{fr} are included for reference. By 3 ps, the Raman spectrum is nearly identical to that of the ground state photoproduct P_{fr}, proving that the isomerization is complete, and that the isomerization occurs on the excited state surface. Right: depiction of the twisting C-D rings during the isomerization reaction.

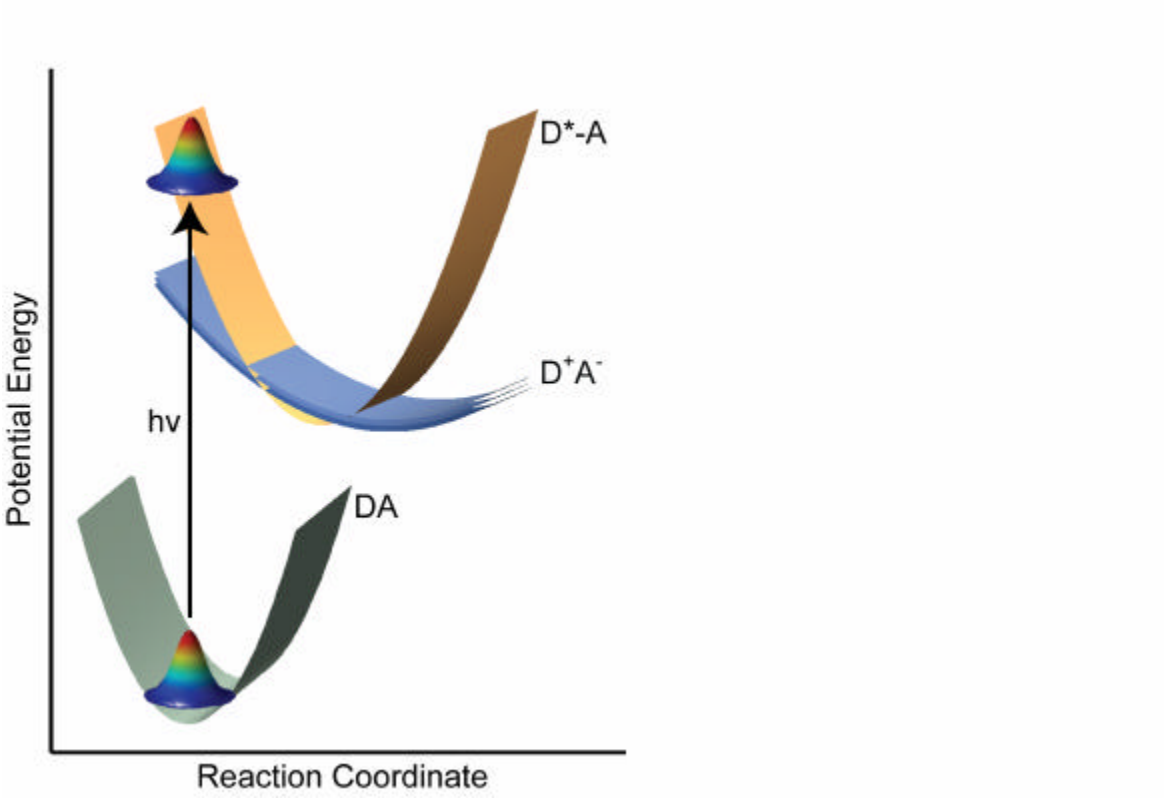

Figure 4. Schematic representation of electron donation from a dye sensitizer into the conduction band of a semiconductor. The ultrafast multidimensional motions which drive the wavepacket down the D*-A acceptor region and promote electron transfer can be elucidated by a high time resolution vibrational structure technique such as FSRS.[31]

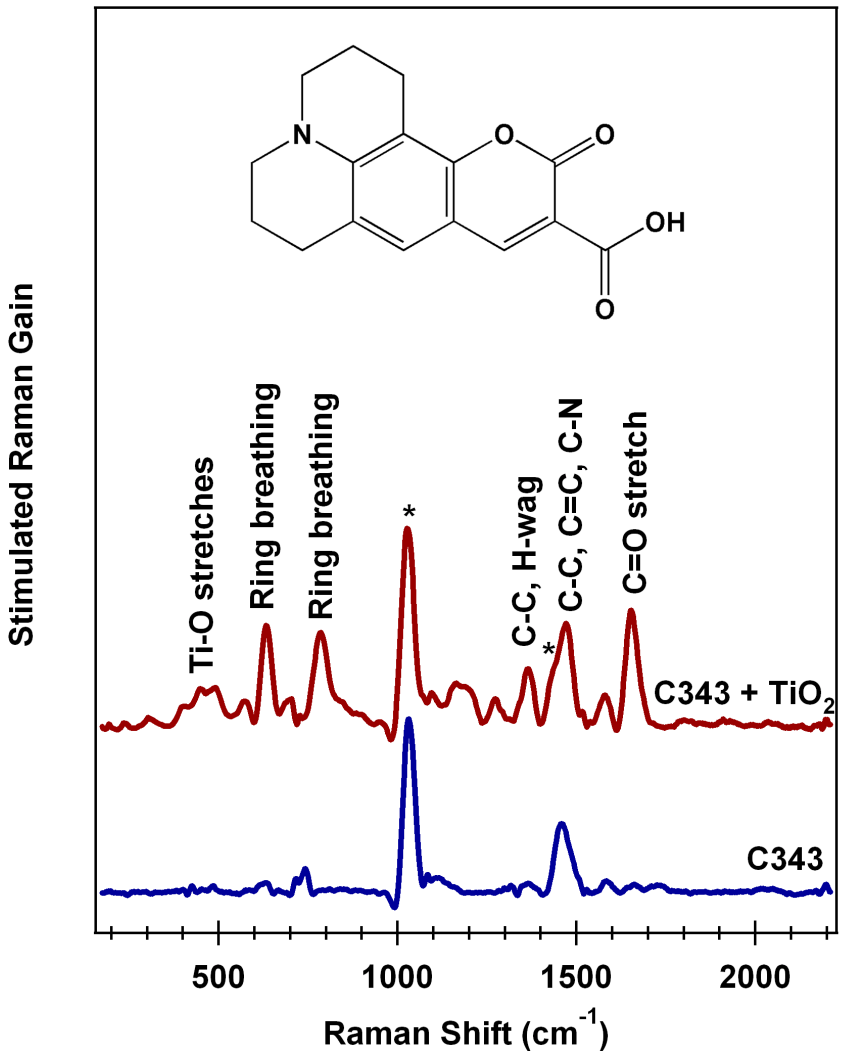

Figure 5. Resonance FSRS of the Coumarin 343 – TiO_2 charge transfer complex and of the unbound Coumarin 343 (C343) dye in methanol. The rich resonance spectrum of the conjugate shows that a large number of vibrational modes contribute to initial motion out of the excited state Franck-Condon region. Additionally, direct binding between the dye molecule and the nanoparticle can be sensed by the large cluster of modes at 500 cm^{-1} including Ti-O stretching. These modes are enhanced on resonance due to the orbital overlap between the dye and nanoparticle. Modes are assigned by comparison to DFT calculations, and solvent features are denoted by an asterisk.

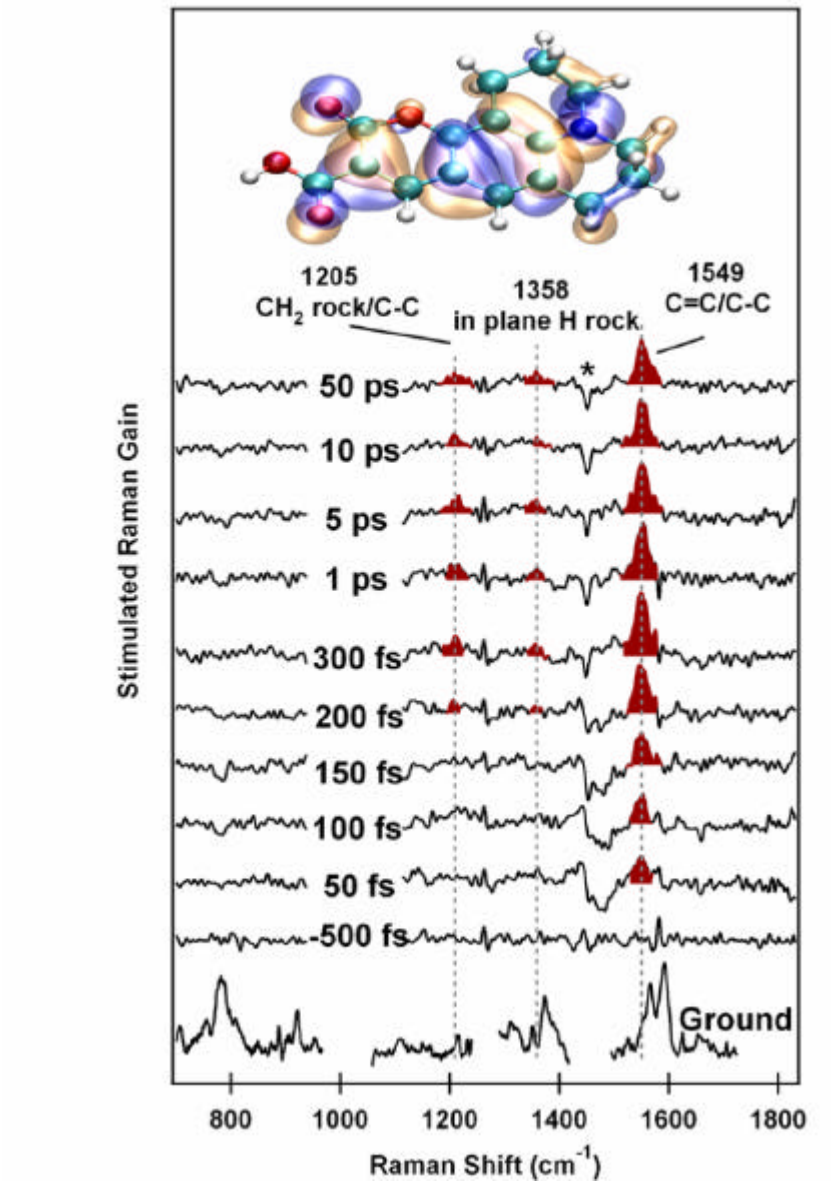

Figure 6. Time-resolved FSRS spectra of the electron injection process in the Coumarin 343-TiO_2 complex. The radical cation with overlaid singly occupied molecular orbital is displayed at the top of the figure, and modes are assigned by comparison with DFT calculations. The time-resolved data reveal the appearance of the radical cation following photoexcitation. The structure does not change significantly on the many picosecond timescale.

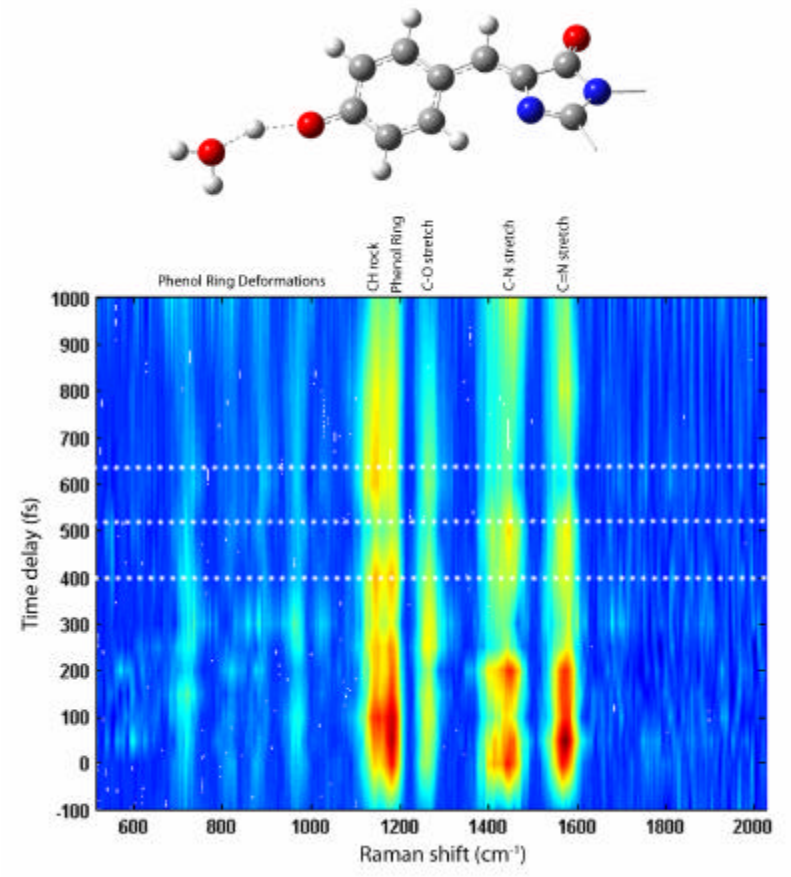

Figure 7. 2D FSRS plot of the time-dependent excited state spectra of wild-type GFP in D_2O. Out of phase intensity modulations are observed for modes on the phenolic ring (the phenol C-H rocking motions at 1145 and 1190 cm^{-1}) and the imidizolinone ring (the C-N and C=N stretches at 1405, 1450, and 1565 cm^{-1}). These oscillations occur with a period of ~280 fs (frequency of ~120 cm^{-1}).

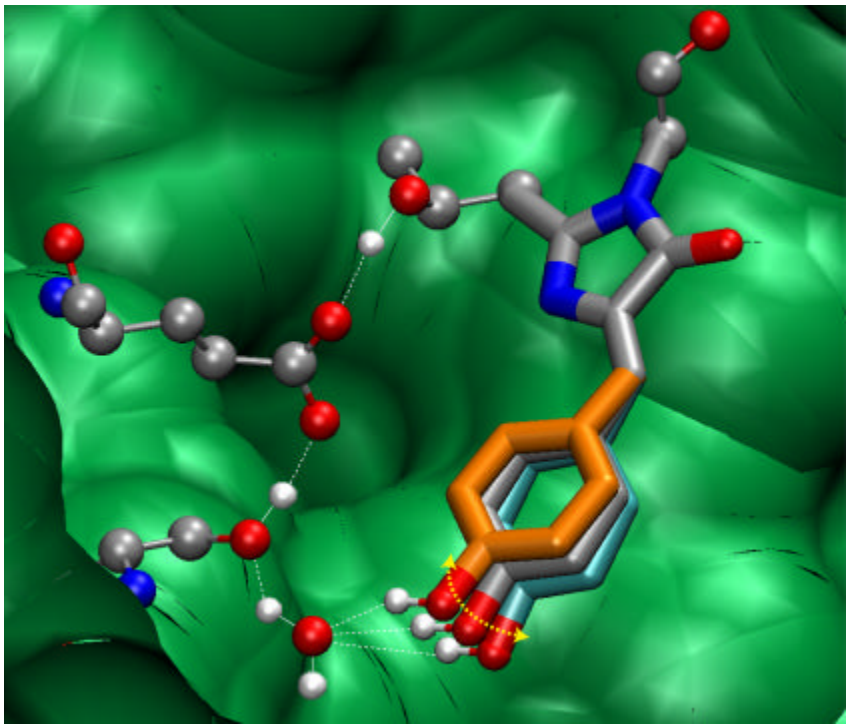

Figure 8. The 120 cm^{-1} (280 fs) vibrational mode driving proton transfer on GFP's excited state surface. As the out-of-plane ring wagging motion proceeds, the phenolic proton is brought in and out of proton binding distance with the nearby water molecule, thus facilitating heavy atom rearrangement along the excited state proton transfer chain for the tautomerized form of the chromophore.[18]

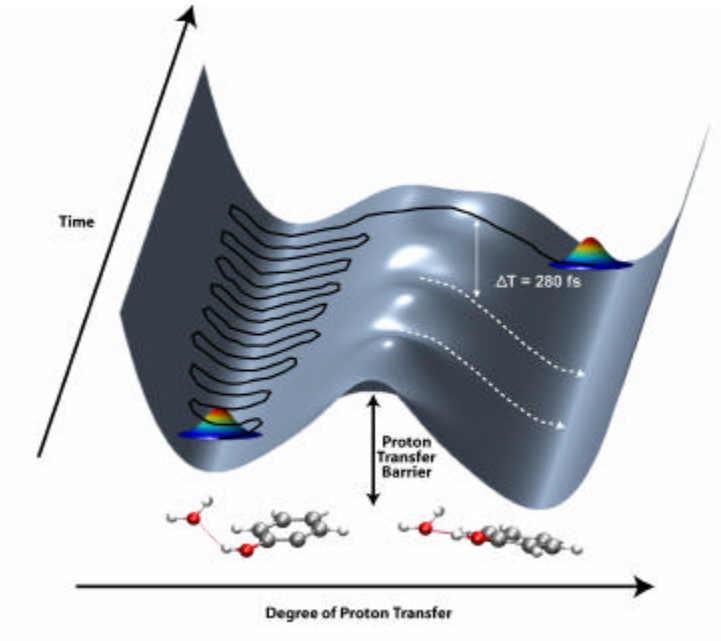

Figure 9. Schematic landscape for the excited state proton transfer in GFP. The low frequency wagging mode, which brings the phenolic ring into better hydrogen bonding alignment with a nearby water molecule, periodically lowers the proton transfer barrier. One possible path for the wavepacket is depicted in black.

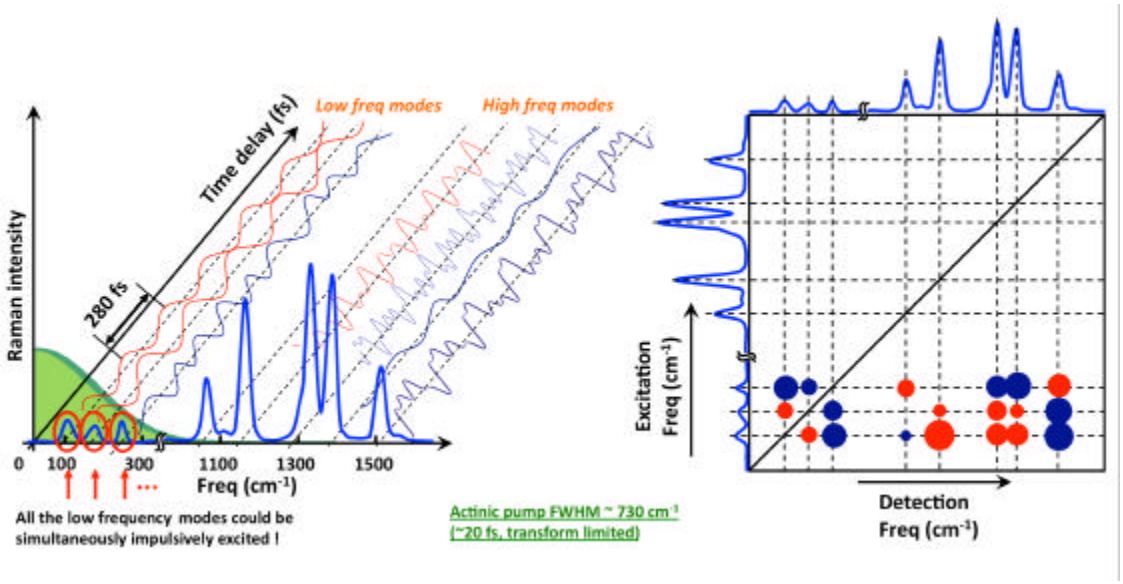

Figure 10. Pictorial representation of short-pulse FSRS. Left: By using sub 10 fs pulses, wavepackets would be excited coherently in all heavy atom modes, which would create numerous oscillations in frequency and intensity amongst all coupled modes. Right: Fourier transform analysis of such data would lead to knowledge of all mode-specific couplings as a function of time, thus determining the complete anharmonicity matrix that makes up a multidimensional reaction coordinate. The blue and red dots denote oppositely phased couplings in this schematic experiment, while the size denotes the strength of the coupling.

Acknowledgements

We would like to thank Rosalie Tran, Keenan Taylor, and J. Clark Lagarias for their many contributions to the experiments and discussions presented here, and the Mathies Royalty Fund for financial support.

References:

1. J. Henin, G. Fiorin, C. Chipot and M. L. Klein, *J. Chem . Theo. Comp.*, 2010, **6**, 35-47.
2. Y. D. Wu, J. D. Schmitt and R. Car, *J. Chem. Phys.*, 2004, **121**, 1193-1200.
3. A. M. Virshup, C. Punwong, T. V. Pogorelov, B. A. Lindquist, C. Ko and T. J. Martinez, *J. Phys. Chem. B*, 2009, **113**, 3280-3291.
4. B. G. Levine and T. J. Martinez, *Annu. Rev. Phys. Chem.*, 2007, **58**, 613-634.
5. P. Kukura, D. W. McCamant and R. A. Mathies, *Annu. Rev. Phys. Chem.*, 2007, **58**.
6. D. W. McCamant, P. Kukura, S. Yoon and R. A. Mathies, *Rev. Sci. Instrum.*, 2004, **75**, 4971-4980.
7. J. V. Lockard, A. B. Ricks, D. T. Co and M. R. Wasielewski, *J. Phys. Chem. Lett.*, 2010, **1**, 215-218.
8. M. Yoshizawa, H. Aoki and H. Hashimoto, *Bull. Chem. Soc. Japan*, 2002, **75**, 949-955.
9. D. W. McCamant, P. Kukura and R. A. Mathies, *J. Phys. Chem. A*, 2003, **107**, 8208-8214.
10. R. R. Frontiera and R. A. Mathies, *Laser and Photonics Reviews*, 2011, **5**, 102-113.
11. S. Y. Lee, D. H. Zhang, D. W. McCamant, P. Kukura and R. A. Mathies, *J. Chem. Phys.*, 2004, **121**, 3632-3642.
12. Z. G. Sun, J. Lu, D. H. Zhang and S. Y. Lee, *J. Chem. Phys.*, 2008, **128**.
13. R. R. Frontiera, S. Shim and R. A. Mathies, *J. Chem. Phys.*, 2008, **129**.
14. E. Ploetz, S. Laimgruber, S. Berner, W. Zinth and P. Gilch, *Appl. Phys. B*, 2007, **87**, 389-393.
15. A. Weigel and N. P. Ernsting, *J. Phys. Chem. B*, 2010, **114**, 7879-7893.
16. J. Dasgupta, R. R. Frontiera, K. C. Taylor, J. C. Lagarias and R. A. Mathies, *Proc. Natl. Acad. Sci. USA*, 2009, **106**, 1784-1789.
17. R. R. Frontiera, J. Dasgupta and R. A. Mathies, *J. Am. Chem. Soc.*, 2009, **131**, 15630-15632.
18. C. Fang, R. R. Frontiera, R. Tran and R. A. Mathies, *Nature*, 2009, **462**, 200-204.
19. S. Mukamel and J. D. Biggs, *J. Chem. Phys.*, 2011, **134**.
20. D. W. McCamant, *J. Phys. Chem. B*, 2011, **115**, 9299-9305.
21. D. W. McCamant, P. Kukura and R. A. Mathies, *J. Phys. Chem. B*, 2005, **109**, 10449-10457.
22. S. Shim, J. Dasgupta and R. A. Mathies, *J. Am. Chem. Soc.*, 2009, **131**, 7592-7597.
23. P. Kukura, D. W. McCamant, S. Yoon, D. B. Wandschneider and R. A. Mathies, *Science*, 2005, **310**, 1006-1009.
24. P. Kukura, D. W. McCamant and R. A. Mathies, *J. Phys. Chem. A*, 2004, **108**, 5921-5925.
25. N. C. Rockwell, Y. S. Su and J. C. Lagarias, *Annu. Rev. Plant Bio.*, 2006, **57**, 837-858.
26. A. J. Fischer and J. C. Lagarias, *Proc. Natl. Acad. Sci. USA*, 2004, **101**, 17334-17339.

27. S. Laimgruber, W. J. Schreier, T. Schrader, F. Koller, W. Zinth and P. Gilch, *Angew. Chem.-Int. Ed.*, 2005, **44**, 7901-7904.
28. R. A. Marcus and N. Sutin, *Biochim. Biophys. Acta*, 1985, **811**, 265-322.
29. J. Jortner and M. Bixon, *J. Chem. Phys.*, 1988, **88**, 167-170.
30. B. Oregan and M. Gratzel, *Nature*, 1991, **353**, 737-740.
31. R. Huber, J. E. Moser, M. Gratzel and J. Wachtveitl, *Chem. Phys.*, 2002, **285**, 39-45.
32. H. N. Ghosh, J. B. Asbury and T. Q. Lian, *J. Phys. Chem. B*, 1998, **102**, 6482-6486.
33. J. B. Asbury, E. Hao, Y. Q. Wang, H. N. Ghosh and T. Q. Lian, *J. Phys. Chem. B*, 2001, **105**, 4545-4557.
34. A. B. Myers, *Chem. Phys.*, 1994, **180**, 215-230.
35. A. B. Myers, *Chem. Rev.*, 1996, **96**, 911-926.
36. R. L. Blackbourn, C. S. Johnson, J. T. Hupp, M. A. Bryant, R. L. Sobocinski and J. E. Pemberton, *J. Phys. Chem.*, 1991, **95**, 10535-10537.
37. S. K. Doorn and J. T. Hupp, *J. Am. Chem. Soc.*, 1989, **111**, 1142-1144.
38. M. Chalfie, Y. Tu, G. Euskirchen, W. W. Ward and D. C. Prasher, *Science*, 1994, **263**, 802-805.
39. M. Ormo, A. B. Cubitt, K. Kallio, L. A. Gross, R. Y. Tsien and S. J. Remington, *Science*, 1996, **273**, 1392-1395.
40. O. Shimomura, *Febs Letters*, 1979, **104**, 220-222.
41. F. Yang, L. G. Moss and G. N. Phillips, Jr., *Nat. Biotechnol.*, 1996, **14**, 1246-1251.
42. M. Chattoraj, B. A. King, G. U. Bublitz and S. G. Boxer, *Proc. Natl. Acad. Sci. USA*, 1996, **93**, 8362-8367.
43. H. Lossau, A. Kummer, R. Heinecke, F. Pollinger-Dammer, C. Kompa, G. Bieser, T. Jonsson, C. M. Silva, M. M. Yang, D. C. Youvan and M. E. Michel-Beyerle, *Chem. Phys.*, 1996, **213**, 1-16.
44. H. Niwa, S. Inouye, T. Hirano, T. Matsuno, S. Kojima, M. Kubota, M. Ohashi and F. I. Tsuji, *Proc. Natl. Acad. Sci. USA*, 1996, **93**, 13617-13622.
45. N. M. Webber, K. L. Litvinenko and S. R. Meech, *J. Phys. Chem. B*, 2001, **105**, 8036-8039.
46. K. Winkler, J. Lindner, V. Subramaniam, T. M. Jovin and P. Vohringer, *Phys. Chem. Chem. Phys.*, 2002, **4**, 1072-1081.
47. D. Mandal, T. Tahara and S. R. Meech, *J. Phys. Chem. B*, 2004, **108**, 1102-1108.
48. D. Stoner-Ma, A. A. Jaye, P. Matousek, M. Towrie, S. R. Meech and P. J. Tonge, *J. Am. Chem. Soc.*, 2005, **127**, 2864-2865.
49. D. Stoner-Ma, E. H. Melief, J. Nappa, K. L. Ronayne, P. J. Tonge and S. R. Meech, *J. Phys. Chem. B*, 2006, **110**, 22009-22018.
50. P. Kukura, R. Frontiera and R. A. Mathies, *Phys. Rev. Lett.*, 2006, **96**, 238303.
51. R. R. Frontiera and R. A. Mathies, *J. Chem. Phys.*, 2007, **127**.
52. K. C. Wilson, B. Lyons, R. Mehlenbacher, R. Sabatini and D. W. McCamant, *J. Chem. Phys.*, 2009, **131**.
53. R. D. Mehlenbacher, B. Lyons, K. C. Wilson, Y. Du and D. W. McCamant, *J. Chem. Phys.*, 2009, **131**.
54. Z. G. Sun, B. N. Fu, D. H. Zhang and S. Y. Lee, *J. Chem. Phys.*, 2009, **130**.

55. A. Tokmakoff and G. R. Fleming, *J. Chem. Phys.*, 1997, **106**, 2569-2582.
56. K. Tominaga and K. Yoshihara, *J. Chem. Phys.*, 1996, **104**, 4419-4426.
57. S. Saito and I. Ohmine, *J. Chem. Phys.*, 1998, **108**, 240-251.
58. K. Tominaga and K. Yoshihara, *Phys. Rev. Lett.*, 1995, **74**, 3061-3064.
59. D. A. Blank, L. J. Kaufman and G. R. Fleming, *J. Chem. Phys.*, 1999, **111**, 3105-3114.
60. A. Kahan, O. Nahmias, N. Friedman, M. Sheves and S. Ruhman, *J. Am. Chem. Soc.*, 2007, **129**, 537-546.
61. D. Polli, L. Luer and G. Cerullo, *Rev. Sci. Instrum.*, 2007, **78**.
62. H. Eyring and M. Polanyi, *Zeitschrift Fur Physikalische Chemie-Abteilung B-Chemie Der Elementarprozesse Aufbau Der Materie*, 1931, **12**, 279-311.
63. H. Eyring, *Chem. Rev.*, 1932, **10**, 103-123.
64. H. Pelzer and E. Wigner, *Zeitschrift Fur Physikalische Chemie-Abteilung B-Chemie Der Elementarprozesse Aufbau Der Materie*, 1932, **15**, 445-471.
65. W. Humphrey, A. Dalke and K. Schulten, *J. Molec. Graphics*, 1996, **14**, 33-38.